EXPERIMENTAL SIMULATION OF A DIRECT VESSEL INJECTION LINE BREAK OF THE APR1400 WITH THE ATLAS

KI-YONG CHOI*, HYUN-SIK PARK, SEOK CHO, KYOUNG-HO KANG, NAM-HYUN CHOI, DAE-HUN KIM, CHOON-KYUNG PARK, YEON-SIK KIM and WON-PIL BAEK
Thermal Hydraulics Safety Research Division, Korea Atomic Energy Research Institute
1045 Daedeokdaero, Yuseong, Daejeon, 305-353, Korea
*Corresponding author. E-mail : kychoi@kaeri.re.kr

Received September 2, 2008
Accepted for Publication January 2, 2009

The first-ever integral effect test for simulating a guillotine break of a DVI (Direct Vessel Injection) line of the APR1400 was carried out with the ATLAS (Advanced Thermal-hydraulic Test Loop for Accident Simulation) from the same prototypic pressure and temperature conditions as those of the APR1400. The major thermal hydraulic behaviors during a DVI line break accident were identified and investigated experimentally. A method for estimating the break flow based on a balance between the change in RCS inventory and the injection flow is proposed to overcome a direct break low measurement deficiency. A post-test calculation was performed with a best-estimate safety analysis code MARS 3.1 to examine its prediction capability and to identify any code deficiencies for the thermal hydraulic phenomena occurring during the DVI line break accidents. On the whole, the prediction of the MARS code shows a good agreement with the measured data. However, the code predicted a higher core level than did the data just before a loop seal clearing occurs, leading to no increase in the peak cladding temperature. The code also produced a more rapid decrease in the downcomer water level than was predicted by the data. These observable disagreements are thought to be caused by uncertainties in predicting countercurrent flow or condensation phenomena in a downcomer region. The present integral effect test data will be used to support the present conservative safety analysis methodology and to develop a new best-estimate safety analysis methodology for DVI line break accidents of the APR1400.

KEYWORDS : ATLAS, DVI Line Break, SB-LOCA, APR1400

1. INTRODUCTION

1.1 Background

KAERI (Korea Atomic Energy Research Institute) has been operating an integral effect test facility, the ATLAS (Advanced Thermal-Hydraulic Test Loop for Accident Simulation) for accident simulations for the OPR1000 and the APR1400, which are in operation and under construction in Korea, respectively [1,2]. The simulation capability of the ATLAS for major DBAs (Design Basis Accidents), including a large-break loss-of-coolant, a direct vessel injection line-break, and a main-steam-line-break accident, was evaluated by a best-estimate system code MARS [3]. It was revealed that the ATLAS has enough capability to simulate major DBAs for the APR1400.

The ATLAS program started in 1997 under a nuclear R&D mid- and long-term project funded by the Korean government. Since the complete installation of the ATLAS in 2005, several commissioning tests have been successfully performed [4]. Subsequently, the first preliminary integral effect test for a small break LOCA (SBLOCA) with a break size equivalent to a 3-inch cold leg break was performed in 2006 [5]. Comparison of the measured data and the post-test calculation results contributed to characterizing the integral behavior of the ATLAS. The achieved integral data was also used to minimize the scaling distortion of the ATLAS and to improve the input model of the ATLAS for the MARS code.

In 2007, the ATLAS was extensively used for a broad range of integral tests on the reflood phase of a large break LOCA (LBLOCA) in order to resolve two safety issues of the APR1400 raised by a regulatory organization during its licensing process. One safety issue is the ECC (Emergency Core Cooling) bypass phenomenon in the upper annulus downcomer; the other is the downcomer

boiling phenomenon in the lower annulus downcomer during the reflood phase for a postulated large break LOCA [2,6]. More than fifteen tests have been completed to support resolution of the safety issues; an intensive code assessment project is under way in collaboration with several organizations such as KINS (Korea Institute of Nuclear Safety), KNF (Korea Nuclear Fuel Co., Ltd.), and KHNP (Korea Hydro & Nuclear Power Co., Ltd.). Afterwards, at the beginning of 2008, the ATLAS was modified to have a configuration enabling simulation of DVI line break accidents of the APR1400.

1.2 DVI Line Break

The AP600 (or the AP1000) was the first reactor to adopt a DVI method for an emergency core cooling system. The double-ended severance of a DVI line is taken as a limiting sequence for an SBLOCA analysis of the AP1000. The US-APWR also selected the DVI method for delivering borated ECC water from safety injection pumps into the core. The DVI nozzle is located below the elevation of the centerline of the hot leg and cold leg nozzles. The VVER-1000 passively injects borated water from four pressurized accumulation tanks into the reactor core through separate inlet nozzles attached to the reactor pressure vessel (RPV). Those DVI-adopted plants treat a DVI line break as another instance along a spectrum of SBLOCAs in their safety analysis because, from a safety viewpoint, a DVI nozzle directly attached to a reactor vessel is vulnerable to a postulated break.

The APR1400 also adopted the DVI method as an improved safety feature; the DVI nozzles are located 2.1m above the cold leg. This new design feature of the APR1400 can eliminate complicated piping interconnections and is believed to ensure that more safety injection water reaches the reactor core. As the DVI line is an inherent design feature of the APR1400, a postulated accident, in which a DVI line may be broken, should be taken into account as one of the SB-LOCAs to ensure the safety of the APR1400. As the DVI nozzle, of which the inner diameter is 8.5 inches, is located in the upper part of the reactor pressure vessel downcomer, it seems that the thermal hydraulic phenomena in the RPV downcomer may be different from those in the cold leg injection (CLI) mode during design basis accidents [7]. In the event of a DVI line break, the vapor generated in the core is introduced into the RPV downcomer through the hot legs, the steam generators, and the cold legs. Then, the vapor should pass through the upper part of the RPV downcomer to be discharged through the broken DVI nozzle. Therefore, the behavior of the two-phase flow in the upper annulus downcomer is expected to be complicated and relevant models need to be implemented into the safety analysis codes in order to predict these thermal hydraulic phenomena correctly [8].

The URD (Utility Requirement Document) published by the EPRI (Electric Power Research Institute) recommends that a core uncovery should be prevented for an SB-LOCA up to an equivalent break diameter of 6 inches by a best-estimate thermal-hydraulic analysis [9]. The PSAR (Preliminary Safety Analysis Report) for the APR1400 includes safety analysis results for DVI line break accidents [10]. The safety analysis was performed by the CEFLASH-4AS code, which is based on a conservative evaluation model (EM). Four different break sizes were analyzed: 100%, 25%, 12.5%, and 5% of the cross section of an 8.5 inch DVI nozzle. For all the cases, the predicted peak cladding temperatures (PCT) were much lower than values in the acceptance criterion specified in 10 CFR 50.46, even though a partial core uncovery is predicted for break sizes greater than 25% of the cross section of the DVI nozzle.

Bae et al. [11] performed sensitivity studies on DVI line break size with a modified CEFLASH-4AS/REM code as a best-estimate approach. They showed that the DVI line breaks for an equivalent break diameter greater than six inches experience a core uncovery and consequently a fuel heatup. However, the predicted PCT is well below the acceptance criterion of 10 CFR 50.46. Chung et al. [12] carried out a PIRT (Phenomena Identification and Ranking Tabulation) for an identification of the important thermal-hydraulic phenomena during a DVI line break in the APR1400. The panel agreed that the scenario should be partitioned into four time phases: pre-trip, post-trip, refill, and long term cooling phases. The high ranked phenomena with a poor knowledge level, which are important for the uncertainty of a code model and further experimental work, were identified as follows: (1) cold leg to downcomer break flow, (2) countercurrent flow in a downcomer, (3) fluidic device flow during an SBLOCA, and (4) condensation in a downcomer. Recently, the SNUF (Seoul National University Facility) was utilized to simulate a DVI line break accident [13]. It was observed that the downcomer seal clearing phenomena had a dominant role in the decrease of system pressure and an increase of coolant level of the core. However, the SNUF is an RHRP (Reduced Height and Reduced Pressure) facility, which cannot be operated at a higher pressure than 0.8MPa; it has a limited simulation capability due to its low core power and the fact that the secondary system is simplified as a lumped boundary condition. So far there is not enough integral effect test data for DVI line breaks that can demonstrate the progression of a DVI line break accident realistically and can be used for a code assessment and improvement.

1.3 Objectives

Sensitivity tests on DVI line break sizes are now underway with the ATLAS. Four break sizes, 100%, 50%, 25% and 5% of the cross section of a DVI nozzle are intended to be investigated experimentally. For the first DVI line break test, a guillotine break test of a DVI nozzle was carried out and the test was denoted for convenience

as SB-DVI-08. One of the objectives of the present test is to obtain integral effect test data for a 100% break of a DVI nozzle at well-defined experimental conditions; results can be used to enhance our understanding of thermal hydraulic behavior during the transient phases in PIRT. The last phase, a long term cooling phase, is excluded in the present investigation. This paper explains how the initial and boundary conditions for the present integral effect test are determined from a scaling viewpoint. The transient behaviors of the major thermal hydraulic parameters during the test period will be explained.

Safety analysis methodology or the safety analysis code itself used for the analysis of DVI line break accidents needs to be validated with a comprehensive, integral database. In particular, a best-estimate safety analysis methodology for DVI line break accidents needs to be developed to identify uncertainties involved in the present conservative safety analysis. Such best-estimate safety analysis methodology will contribute to defining a more precise specification of safety margins and thus lead to a greater operational flexibility. However, such an effort has never been reported because of the lack of an integral database on DVI line break accidents. Therefore, another objective of the present work is to assess the code modeling capabilities and to identify any deficiencies of best-estimate system codes against the obtained integral data on DVI line break accidents. In the present work, the MARS 3.1 code was used as a best-estimate code. A post-test calculation was performed based on the obtained experimental boundary conditions with the MARS code. The prediction capability of the MARS code for the major thermal hydraulic behaviors is investigated and the effects of various input uncertainties on the calculation results are discussed.

2. DESCRIPTION OF THE ATLAS

The ATLAS has the same two-loop features as the APR1400 and is designed according to the well-known scaling method suggested by Ishii and Kataoka [14] to simulate the various test scenarios as realistically as possible. It is a half-height and 1/288-volume scaled test facility with respect to the APR1400. The main motive for adopting the reduced-height design is to allow for an integrated annular downcomer in which the multidimensional phenomena can be important in some accident conditions with a DVI operation. According to the scaling law, the reduced height scaling has time-reducing results in the model. For the one-half-height facility, the time for the scaled model is $\sqrt{2}$ times faster than prototypical time. The friction factors in the scaled model are maintained at

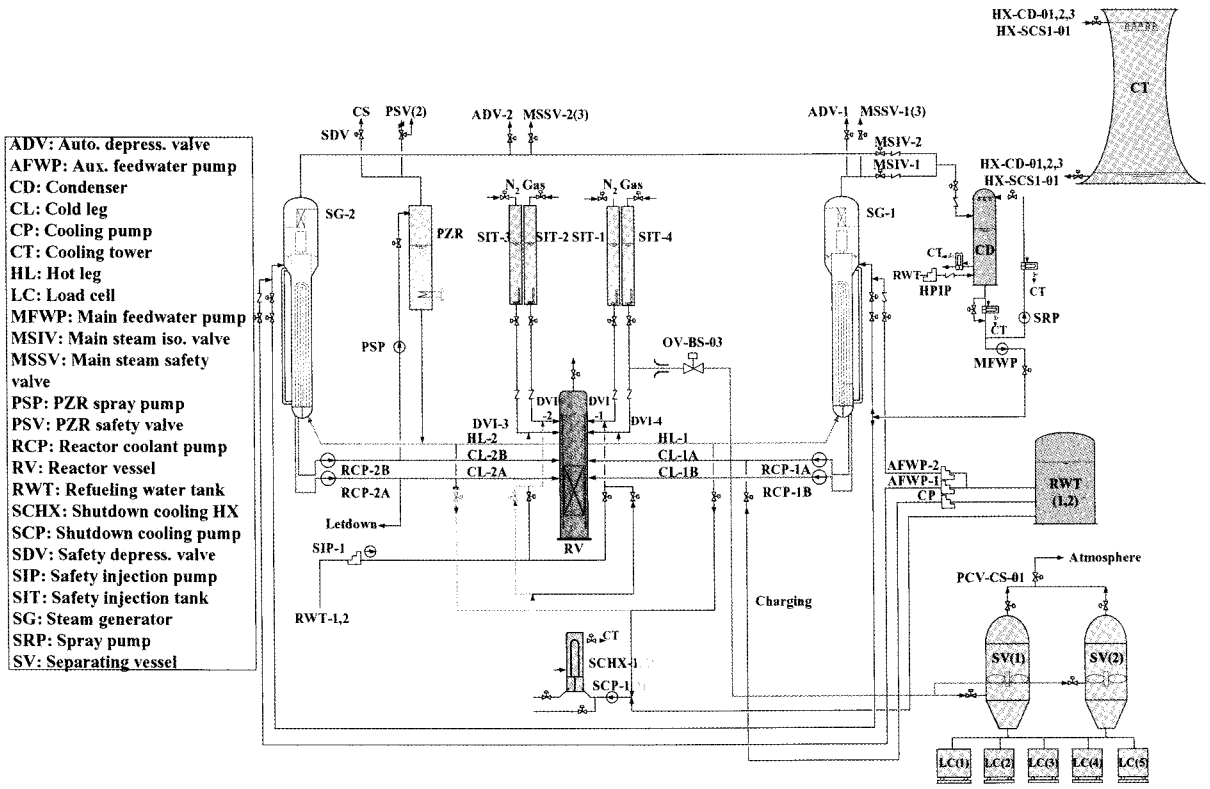

Fig. 1. Schematics of the Overall ATLAS

the same levels as those of the prototype. The hydraulic diameter of the scaled model is maintained the same as that of the prototype to preserve the prototypical conditions for the heat transfer coefficient.

The fluid system of the ATLAS consists of a primary system, a secondary system, a safety injection system, a break simulating system, a containment simulating system, and auxiliary systems. The primary system includes a reactor vessel, two hot legs, four cold legs, a pressurizer, four reactor coolant pumps, and two steam generators. The secondary system of the ATLAS is simplified to be of a circulating loop-type. The steam generated by the two steam generators is condensed in a direct condenser tank and the condensed feedwater is again injected into the steam generators. Most of the safety injection features of the APR1400 and the OPR1000 are incorporated into the safety injection system of the ATLAS, which consists of four safety injection tanks (SITs) and a high pressure injection pump that can simulate several operation modes such as charging, letdown, auxiliary spray, pre-heating, safety injection, long-term cooling, and recirculation operations. The break simulating system consists of a quick opening valve, a break nozzle, and instruments. It is precisely manufactured to have a scaled break flow through it in the case of the LOCA tests. The containment simulating system of the ATLAS has a function of collecting the break flow rate and maintaining a specified pressure in order to simulate containment. Besides, the ATLAS has auxiliary systems such as a shutdown cooling system, a makeup system, a component cooling system, a nitrogen/air/steam supply system, a vacuum system, and a heat tracing system. A schematic diagram of the overall ATLAS for the present DVI line break test is shown in Fig. 1. Detailed ATLAS design and a description of the ATLAS development program can be found in the literature [15].

3. EXPERIMENTAL CONDITIONS

The present experimental conditions were determined by a pre-test calculation with a best-estimate thermal hydraulic code, MARS 3.1. First of all, a transient calculation was performed for the DVI line break of the APR1400 to obtain the reference initial and boundary conditions. A best-estimate safety analysis methodology, which is now commonly accepted in nuclear industries, was applied to the transient calculation of the APR1400. The safety injection system of the APR1400 has four mechanically separated hydraulic trains. They are also electrically separated by two divisions, implying that each emergency diesel generator powers two hydraulic trains. The pre-test calculation was conducted with the assumption of loss of off-site power simultaneously with the break and the worst single failure as a loss of a diesel generator, resulting in the minimum safety injection flow to the core. Furthermore, the safety injection flow to the broken DVI-4 nozzle was not credited. Therefore, the safety injection flow from the safety injection pump (SIP) is only injected through the DVI-2 nozzle opposite to the broken DVI-4 nozzle. As regards the safety injection flow from the four safety injection tanks (SIT), three SITs except for the SIT connected to the broken DVI-4 nozzle are available to provide the safety injection flow into the core. Configuration of the

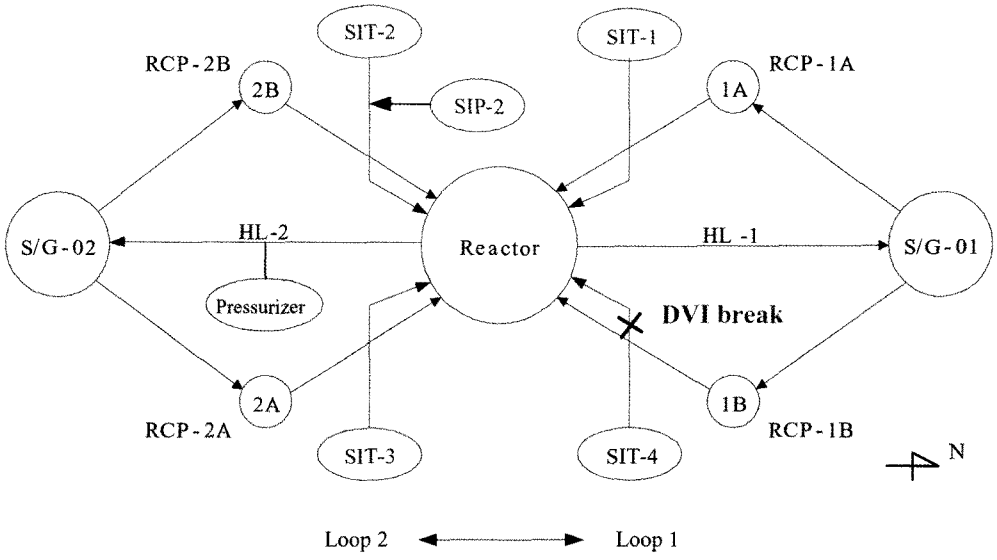

Fig. 2. Arrangement of the Primary Loop of the ATLAS

Table 1. Comparison of the Sequence of Events of the Present Test

Events	APR1400 (time, sec)	ATLAS (time,sec)	Description
Break open	0	0	
Low pressurizer pressure trip (LPP)	20.9		If pressurizer pressure < 10.72MPa
Pressurizer heater trip	LPP+0.0 sec	LPP+0.0 sec	
Reactor scram & RCP trip	LPP+0.5 sec	LPP+0.35 sec	
Turbine isolation	LPP+0.1 sec	LPP+0.07 sec	
Main feedwater isolation	LPP+10 sec	LPP+7.07 sec	
Safety injection pump start	LPP+40 sec	LPP+28.28 sec	
Low upper downcomer pressure trip (LUDP)	LUDP	LUDP	If downcomer pressure < 4.03MPa
Safety injection tank (SIT) start	LUDP+0.0 sec	LUDP+0.0 sec	
Low flow turndown of the SIT	SIT level < ~54%	SIT level < ~54%	If water level of the SIT is less than a specified set point

primary loop together with the arrangement of the ECC systems for the present test is shown in Fig. 2.

A conservative 1973 ANS decay heat curve with a 1.2 multiplication factor was used in the present calculation. It is noteworthy that the containment back-pressure does not affect the progression of the transient in a DVI line break accident, because a choking condition is maintained throughout most of the time phases. Therefore, the containment back-pressure was not controlled and was maintained at atmospheric pressure in the present test.

Based on the calculated sequence of events of the APR1400, the initial and boundary conditions of the present integral effect test were determined. The delay time required for an initiation of the safety injection systems such as the safety injection pump and the safety injection tank was reduced by the square root of two according to the scaling law of the ATLAS. Also, the delay times for the isolation of the secondary feedwater or steam supply systems were also scaled down by the same time scaling ratio of the ATLAS. The detailed sequence of events applied to the present test is summarized in Table 1.

4. MAJOR COMPONENT SCALING

The present integral effect test is performed at the same pressure and temperature conditions as those of the prototype plant, APR1400, especially in the primary system. Compared with the prototypic secondary pressure, the secondary pressure of the ATLAS is slightly reduced to obtain a steady state condition at 8% power level. Otherwise, the primary temperature distribution along the primary loop can be distorted. In order to simulate the transient behavior of the APR1400 during a DVI line break as closely as possible to the ATLAS, the crucial components, whose performance can influence transient behavior, must be appropriately scaled down. The reactor core, the heat loss compensation system, the break nozzle, the safety injection pump, the safety injection tank, and the core bypass flow path were defined as the components of extreme importance.

4.1 Reactor Core

The ATLAS has a maximum power capacity of 8% of the scaled full power. An initial primary condition for the present data was obtained by applying 8% of the scaled power and by reducing the primary coolant flow rate by 8%. This process results in the same temperature distribution along the reactor coolant loop, which can minimize scaling distortion.

Scaling analysis was performed to establish an optimized core power that can minimize the distortion caused by the 8% core power of the ATLAS. Several options were investigated, such as a no-delayed power trip and an additional delayed power trip with the best-estimate MARS 3.1 code. Stored energy of the reactor coolant inventory as well as the heater rod structure was carefully compared between the APR1400 and the ATLAS. It was concluded that the case of the no-delayed power trip, in which the core power maintains a constant value until it intersects with the scaled decay power and then follows the scaled decay power curve, resulted in a better scaling agreement than that in the case of the additional delayed power trip. In the case of the additional delayed power trip, in which the core power maintains a constant value for an additional period after an intersection with the scaled decay power before it starts to follow the scaled power curve, the break flow enthalpy was magnified more than it was in the APR1400, due to the additional applied power. As a

consequence, the core power was programmed to be constant until it intersected with the scaled decay power. Then, the core power was continuously controlled to follow 120% of the ANS73 decay curve throughout the test. As the core of the ATLAS consists of three groups in order to simulate a radial distribution of the reactor power, the power of each group was controlled separately by an SCR (Silicon Controlled Rectifier) to have a uniform power distribution in a radial direction.

4.2 Heat Loss Compensation System

Heat loss to the surroundings is considered to be one of the critical factors affecting transient behavior. Physically, the heat loss rate can be determined by a free convection equation for a given temperature difference between an outer surface temperature and a surrounding temperature. The heat loss rate due to free convection for an arbitrary immersed geometry is proportional to the temperature difference with a power of 5/4 by Lienhard [16] as follows:

$$Q_{loss} \propto \Delta T^{5/4} \tag{1}$$

Separate effect tests were conducted to quantify a heat loss of the ATLAS for a specified wall temperature. The secondary side was filled with air at atmospheric conditions and the pressurizer was isolated from the primary system. As an integral approach, the primary system was heated to a predetermined temperature and maintained at a constant temperature by controlling the core power. When the whole system reaches a steady state condition, the core power supplied at that time can be regarded as a heat loss of the primary system. Based on separate effect test results for various specified temperatures, the following empirical heat loss correlation was developed for the ATLAS.

$$Q_{loss} = 0.32 \cdot (T_w - T_{atm}), \tag{2}$$

where T_w and T_{atm} are representative wall temperature and atmospheric temperature, respectively. During the transient, T_w and T_{atm} were obtained by averaging the measured outer surface temperatures of the downcomer wall of the RPV at three different locations and the atmospheric temperatures surrounding the ATLAS at four distributed locations, respectively. Based on the averaged T_w and T_{atm}, the heat loss rate to the surroundings was estimated by Eq. (2) and was added to the core power. In particular, the estimated heat loss rate from Eq.(2) was partitioned into three groups to make certain of a uniform heat flux distribution of the core power in a radial direction. Though this empirical correlation was obtained at steady state condition, it was assumed that it can be applied to the present transient test to compensate for the heat loss to the surroundings.

4.3 Break Nozzle

A configuration of the break simulation system for the present DVI line break test is shown in Fig. 3. It consists of a quick opening valve, a break nozzle, a case holding the break nozzle, and a few instruments. A pressure transducer and two thermocouples were installed both upstream and downstream of the break nozzle.

Detailed geometry of the break nozzle for the present DVI line break test is shown in Fig. 4. The inner diameter of the break nozzle takes first priority over anything else from the viewpoint of break flow rate scaling. When a break occurs, a choking is expected to occur during the

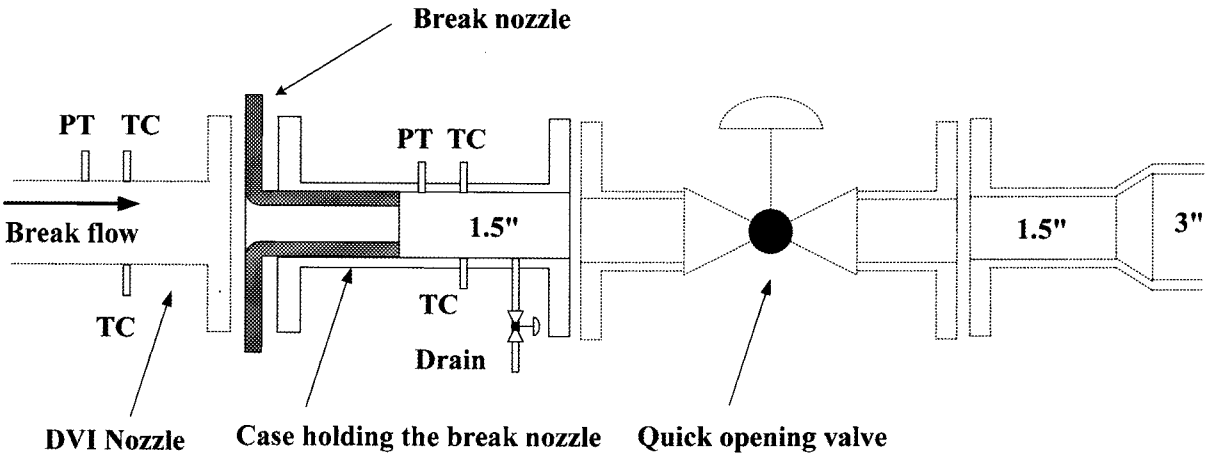

Fig. 3. Configuration of the Break Simulation System for the DVI Line Break Tests

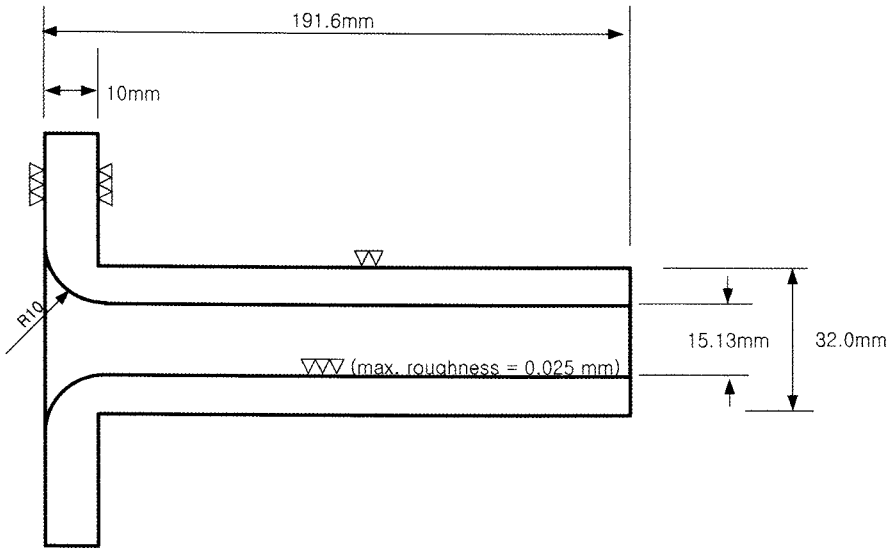

Fig. 4. Detailed Geometry of the Break Nozzle for the Present DVI Line Break Test

entire test period according to the pre-test calculation by the MARS 3.1 code. Therefore, the break area should be scaled down according to the scaling ratio of the flow rate, 1/203.6. The inner diameter of the break nozzle was thus determined to be 15.13mm, which corresponds to 1/203.6 of the 8.5 inch break diameter of the APR1400. The length to diameter ratio of the break nozzle L/D takes the second scaling priority. It was noted that the data obtained for long tubes (12<L/D<40) can be correlated with a model that assumes a thermodynamic equilibrium and that the critical flow rate was relatively insensitive to the L/D for L/D>12.0 [17,18]. Hence, the break nozzle was designed to have a well-rounded entrance and its length was fixed at 191.6 mm including the entrance region to comply with the long pipe requirement that the length to diameter ratio should be above 12. For the chosen nozzle, the scaling ratio of the friction loss coefficient between the reactor pressure vessel and the break point was preserved by controlling the roughness of the break nozzle. Though the friction loss coefficient along the break nozzle, which depends on the roughness of the break nozzle, is considered not to be an influential parameter affecting the break flow rate, the roughness was confirmed in order to carefully comply with a specified requirement during the nozzle fabrication process.

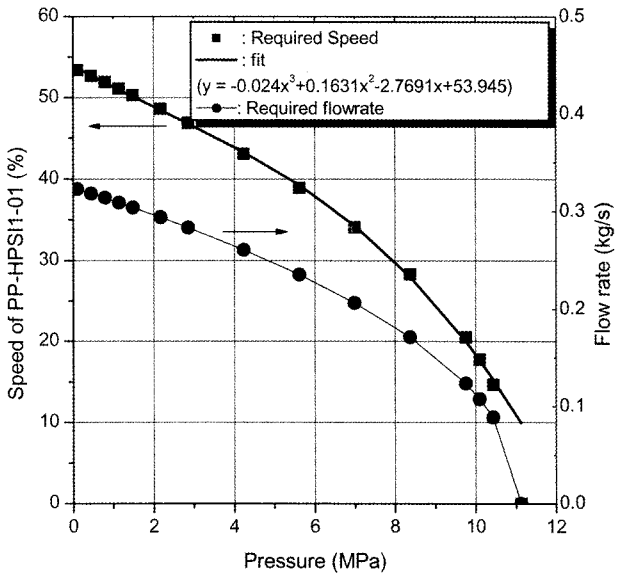

Fig. 5. Required Safety Injection Flow Rate and Corresponding Rotational Speed of the Safety Injection Pump

4.4 Safety Injection Pump

During a DVI line break accident, safety injection water is expected to be supplied by one safety injection pump and three safety injection tanks. According to the pre-test calculation, the safety injection water flow rate of the SI pump is a function of the primary pressure, because the SI pump of the APR1400 is of a centrifugal type. The lower the primary pressure becomes, the larger the SI flow rate becomes. In the ATLAS, a metering type SI pump was installed for greater control flexibility. Its discharge flow rate depends only on the rotational speed for a specified stroke length, regardless of the discharge pressure. The SI pump was equipped with a VVVF (Variable Voltage Variable Frequency) controller to control its rotational speed.

First of all, the pipeline was aligned from the discharge

nozzle of the safety injection pump to the DVI-2 nozzle and then an empirical linear relationship between the SI flow rate and the rotational speed was obtained by a separate effect test. Then, the required SI flow rate as a function of the primary pressure was obtained from the pre-test calculation of the APR1400. As a result, the required rotation speed of the SI pump as a function of the primary downcomer pressure was achieved empirically. This empirical relationship was programmed into the control system of the ATLAS to simulate the scaled safety injection flow rate by the SI pump. Required safety injection flow rate and corresponding rotational speed of the safety injection pump are shown in Fig. 5.

4.5 Safety Injection Tank

Another safety injection flow is provided by three safety injection tanks through the intact DVI nozzles, DVI-1, DVI-2, and DVI-3. The SIT of the APR1400 is equipped with a fluidic device (FD) to utilize its emergency cooling water more effectively than does the OPR1000. The FD passively controls the discharge flow rate into the reactor vessel by changing the flow resistance inside the vortex chamber of the FD [19].

The crucial parameters to be preserved in the present DVI line break test are the nitrogen gas volume of the SIT, the discharged high flow rate before the FD is activated, and the discharged low flow rate when the FD is working. Preservation of the nitrogen gas volume implies a preservation of the pressure of the SIT. The initial nitrogen gas volume was preserved by setting the initial water level of the SIT. The nitrogen gas volume when the FD starts to work can be preserved by specifying a water level set value for the SIT. When the water level reaches the specified set value, the discharged flow rate is switched from a high flow injection mode to a low flow injection mode. For the APR1400 and the ATLAS, an emptying of the SIT should be prevented, so that the nitrogen gas is not injected into the primary system both. The free volume of the SIT of the ATLAS has been designed to be 70% larger than that of the APR1400. Therefore, the minimum water level of the SIT of the ATLAS can be determined to simulate the empty condition of the SIT of the APR1400. A summary of the determined water levels of the SIT is shown in Table 2.

The ATLAS has been slightly modified to simulate such a flow rate switching feature of the FD by installing an orifice and by controlling the flow control valve at the discharge pipeline of the SIT. A basic idea is that the discharged high flow rate is simulated by controlling the flow resistance of the pipe line from the bottom of the SIT to the DVI nozzle; the discharged low flow rate is simulated by controlling the stem position of the flow control valve. Therefore, separate effect tests were carried out to determine the throat diameter of the orifice and the stem positions of the flow control valve. The determined throat diameters of the orifices are summarized in Table 3 along with the stem positions of the flow control valves.

Performances of three SITs were tested with the boundary conditions specified in Tables 2 and 3. The measured SIT injection flow characteristics of the ATLAS SITs were compared with those of the typical SIT of the APR1400 in Fig. 6. The injected flow rate of the APR1400 was calculated based on the typical SIT design data. An initial pressure of 3.93MPa was assumed and the fluidic

Table 2. Water Level Set Points of the SIT to Simulate the FD of the APR1400

Status	SIT water level (%)		
	SIT-1	SIT-2	SIT-3
Initial condition	95.1	94.9	94.2
Fluidic device starts	72.8	72.6	72.0
Fluidic device empties	47.4	47.2	46.6

Table 3. Orifice Diameter and Stem Positions of the Flow Control Valves to Simulate the FD of the APR1400

Parameter	SIT-1	SIT-2	SIT-3
Initial nitrogen gas pressure (MPa)	4.2	4.2	4.2
Orifice diameter (mm)	10.5	10.5	11.2
Valve opening at high flow (%)	100.0	100.0	100.0
Valve opening at low flow (%)	18.0	13.0	24.0

device K-factors for high and low flow conditions were assumed to be 16.0 and 100.0, respectively. In addition, the pressure loss coefficient for a discharge line was assumed to be 9.5. An isentropic condition with a specific heat ratio of 1.4 was used to calculate the variation of the SIT pressure of the APR1400. Concerning the back pressure for the APR1400 calculation, the measured downcomer pressure of the ATLAS was used as a boundary condition. A summary of the parameters used to obtain the flow characteristics of the SIT of the APR1400 is shown in Table 4.

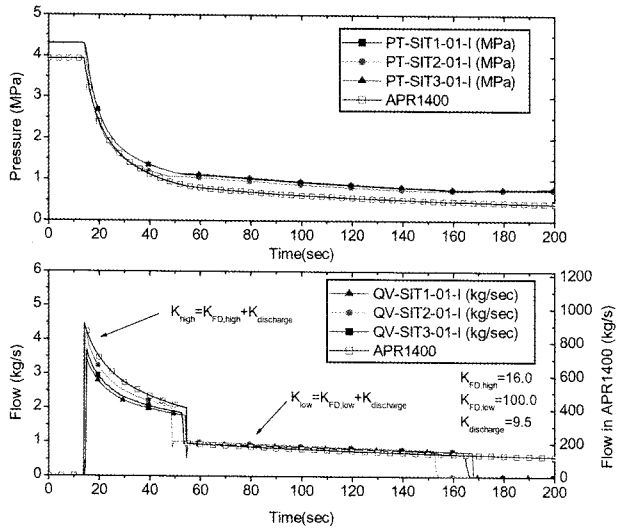

Fig. 6. Performance Characteristics of the SITs of the ATLAS

Table 4. Summary of the Parameters to Obtain the Flow Characteristics of the SIT of the APR1400

Parameter	Value
Initial nitrogen gas pressure (MPa)	3.928
Initial nitrogen gas volume (m^3)	11.19
Initial water volume (m^3)	56.94
Initial water level (m)	11.53
Diameter of the discharge line (m)	0.257
Specific heat ratio (γ)	1.4
Fluidic device K-factor at high flow condition	16.0
Fluidic device K-factor at low flow condition	100.0
Pressure loss coefficient of discharge line (K)	9.5

The top figure of Fig. 6 shows a comparison of the SIT pressure variation during the injection period. The measured trend of the SIT pressure shows a good agreement with the prototypic pressure trend of the APR1400, though the former shows a little higher pressure than that of the APR1400 at low flow conditions. The bottom section of Fig. 6 shows a comparison of the injected flow rate between the ATLAS and the APR1400. The right vertical axis was scaled-up with a 203.6 multiplication factor according to the flow rate scaling ratio of the ATLAS. Overall, the measured data shows good agreement with the characteristics of the SIT of the APR1400. Thus, it can be concluded that the typical characteristics of the SITs of the APR1400 were preserved well in the ATLAS.

4.6 Core Bypass Flow Path

Two kinds of bypass flow paths in the reactor vessel were implemented in the ATLAS. One is the bypass flow path from the downcomer to the hot leg and the other is from the downcomer to the upper head of the core. Each bypass flow path consists of two external pipe lines opposite to each other. A flow control valve was installed at each external pipe line to simulate various bypass flow rates. The flow rates in these bypass flow paths were expected to influence transient behavior during the integral effect tests. Thus, the flow resistances of the bypass flow paths need to be preserved to maintain the same bypass flow characteristics in the ATLAS as in the APR1400. According to pre-test calculations for the APR1400, the downcomer-to-hot leg and downcomer-to-upper head bypass flow rates are 1.4% and 0.5% of the total RCS flow rate, respectively.

Separate effect tests were conducted to determine the openings of the flow control valves to attain the preserved flow resistance of the bypass flow paths. Once the primary coolant flow rate was set to have the scaled flow rate by

Table 5. Required Bypass Flow Rate and Determined Openings of the Bypass Flow Valves

Valves	Bypass flow rate (%)	Bypass flow rate (kg/s)	Valve position (%)
Downcomer to upper head bypass valve, FCV-RV-37	0.25	0.25	74
Downcomer to upper head bypass valve, FCV-RV-38	0.25	0.25	65
Downcomer to hot leg bypass valve FCV-RV-95	0.7	0.71	81
Downcomer to hot leg bypass valve FCV-RV-96	0.7	0.71	97

a full operation of the reactor coolant pump (RCP), the flow rate in each bypass flow path was measured by an external ultrasonic flowmeter for various valve opening positions, from 0% to 100%. As a result, the flow coefficient of the control valve, C_v was obtained experimentally. Based on the obtained flow coefficient of each control valve, each valve's opening position was determined to have the scaled down bypass flow rate through it. The determined valve positions are summarized in Table 5.

5. TEST AND ANALYSIS RESULTS

5.1 MARS Analysis

A one-dimensional model of the MARS 3.1 code was used for a pre-test as well as a post-test analysis of a guillotine break of a DVI line break. First of all, a pre-test analysis for a DVI line break of the APR1400 was carried out to determine the sequence of events (SOE) during the postulated accident. The obtained SOE was applied to the ATLAS system to pre-determine the initial and boundary conditions of the SB-DVI-08 test. Subsequent to the present integral effect test, a post-test analysis was performed based on the obtained data.

Figure 7 shows a nodalization diagram for the present analysis. The same nodalization method was used both for the APR1400 and the ATLAS systems. All the detailed components of the ATLAS were modeled. The core of the ATLAS was modeled with two flow channels: an average and a hot channel core. Each flow channel was modeled as an average rod and a hot rod heat structure. A heated length of 1.905m was modeled with a hydraulic component, PIPE of 20 sub-volumes. All the reactor coolant systems including the reactor vessel, the primary piping, and the reactor coolant pumps were modeled based on the detailed design data of the ATLAS. The annular section of the downcomer was modeled to have six columns that are split azimuthally every 60 °. These columns were also divided by 10 axial nodes, and connected by a cross flow junction component in a circumferential direction to simulate the multi-dimensional flow behavior in a downcomer. The reactor coolant pumps were modeled with homologous data that was obtained from a separate performance test of the reactor coolant pumps installed in the ATLAS [20]. A pressurizer was connected at the intact hot leg. As for the secondary system, two steam generators and main steam lines were modeled. A feedwater system and a turbine system were treated with boundary conditions, and modeled by time dependent volume components. The

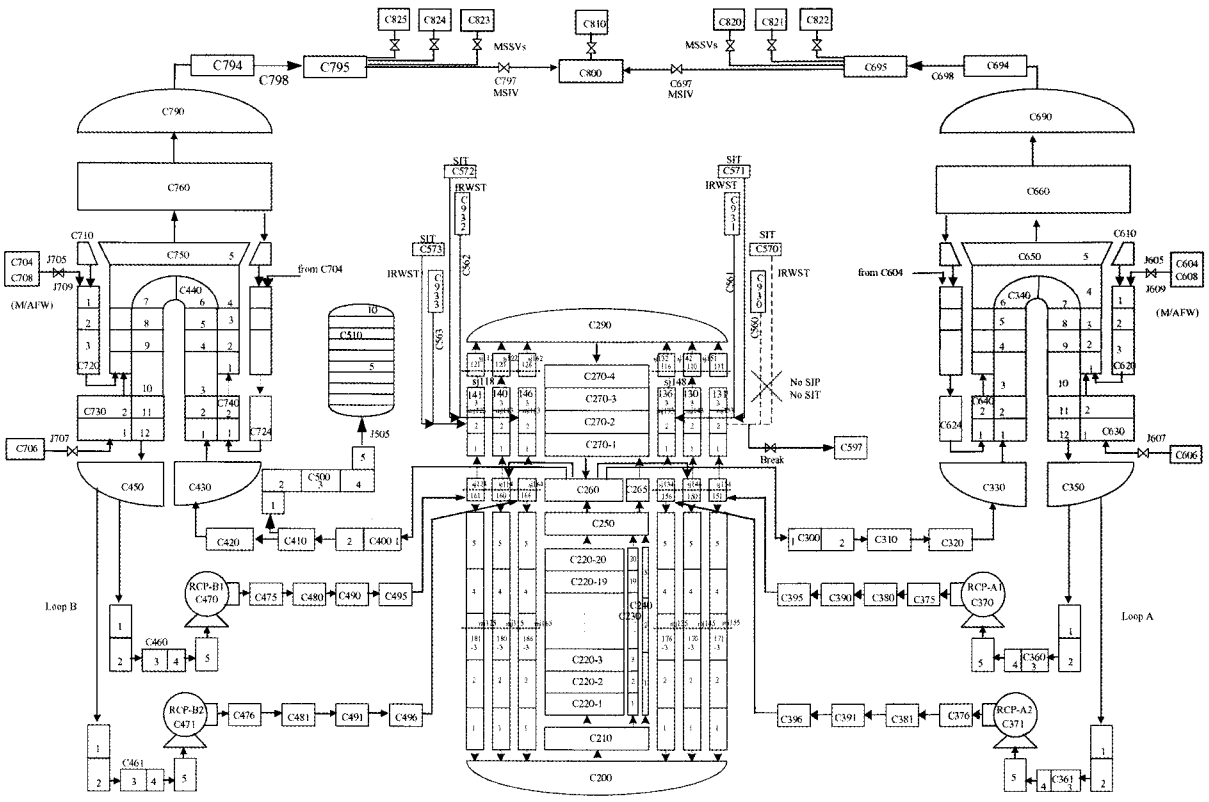

Fig. 7. Nodalization Diagram of the ATLAS for MARS Analysis

safety injection system was also modeled, including four SITs and four SI pumps. Detailed information on the MARS analysis method can be found in the literature [3].

5.2 Steady State Condition

Subsequent to a series of experimental preparation work, a heat-up of the whole system was carried out. During the heat-up process, the primary system was heated with core heaters to its specified steady state condition and this steady state condition was maintained to stabilize the system behavior of the ATLAS. The water inventory in the secondary side of each steam generator was also heated up to a specified temperature of 293.5°C by the heat transferred through the steam generator U-tubes and was pressurized to a specified pressure of 7.83MPa.

When the heat-up process was almost finished, an initialization process was carried out to obtain the required initial and boundary conditions for the DVI line break test throughout the entire system. The pressurizer pressure was controlled to maintain its specified pressure of 15.5MPa. The primary coolant flow rate was reduced to 8% of the scaled value to have the same temperature distribution along the primary loop. It was found that the required 8% of the primary coolant flow rate was achieved in a natural circulation condition in which the speed of the reactor coolant pump was close to zero. The core bypass flow control valves were controlled to have the predetermined stem positions. The secondary system was carefully controlled to maintain a steady state condition of energy balance between the primary and the secondary system. The estimated heat loss was automatically partitioned into three groups to have a uniform heat flux in a radial direction; the partitioned heat loss was added into each heater group by embedded control logics. The initial water levels and pressures of the safety injection tanks were controlled to have the scaled values. The refueling water storage tank (RWT) was filled with water to its initial level of 50% and its water inventory was electrically heated to its pre-determined temperature of 52°C; then, the water was circulated through the bypass injection line so as to preheat the line to the same temperature as the water. The containment pressure control valve was fully opened to simulate atmospheric pressure during the test period. All the connecting pipe lines and three-way valves of the containment simulating system were aligned to measure the break flow rate separately. A comparison of the initial conditions between the specified values and the measured values is shown in Table 6. It can be seen that the measured values for the major parameters are very consistent with the target values, which were determined with a pre-test calculation by the MARS 3.1 code.

Table 6. Comparison of the Initial Conditions for the SB-DVI-08 Test

Parameter	Target value	Measured value	Remarks
Primary system			
- Core power (MW)	1.56	1.647	Initial heat loss: 88kW
- PZR Pressure (MPa)	15.5	15.49	
- Core inlet temp. (°C)	290.7	289.8	
- Core exit temp.(°C)	324.2	324.8	
- RCS flow rate (kg/s)	2.0	2.2	Cold leg averaged value
Secondary system			
- Pressure (MPa)	7.83	7.83/7.83	SG1/SG2
- Steam temp. (°C)	293.5	293.0/293.0	SG1/SG2
- FW temp. (°C)	232.2	232.8/232.8	SG1/SG2
- FW flow rate (kg/s)	0.44	0.323/0.339	SG1/SG2
- Water level (m)	2.0	2.4/2.5	SG1/SG2
- Heat removal (MW)	0.78	0.78	
ECCS			
- SIT pressure (MPa)	4.2	4.23/4.23/4.23	SIT1/SIT2/SIT3
- SIT temp. (°C)	50	51.1/50.8/50.9	SIT1/SIT2/SIT3
- SIT level (m)	95.1/94.9/94.2	95.0/94.6/93.9	SIT1/SIT2/SIT3
- RWT temp. (°C)	50	47.7	RWT1
Containment			
- Pressure (MPa)	0.1	0.1	

5.3 Transient Condition

When a steady state condition was achieved in the whole ATLAS system for more than 10 minutes, a transient DVI line break test was commenced. First of all, a data logging was initiated to log all the measurement points in a steady state condition. After the initial data logging had run for about 200 seconds, the DVI line break test was initiated by opening a quick-opening break valve, OV-BS-03, at the break spool piece. When the pressurizer pressure decreased to the specified pressure of 10.72MPa, a low pressurizer pressure (LPP) signal was generated automatically. The heaters of the pressurizer and all the tracing heaters in the primary system were tripped at the same time as the LPP signal. The RCP was tripped automatically with a time delay of 0.35 seconds after the LPP signal. The main steam and the main feed water line were isolated with a time delay of 0.1 seconds and 7.1 seconds after the LPP signal, respectively. The isolation of the secondary system requires a simultaneous actuation of several valves in the pipe line, which was done by programmed control logic without the operator's intervention. The SI pump was also triggered by the LPP signal, with a time delay of 28.3 seconds. As the initiation of the SI pump also requires an alignment of the valves located in the supply line, this alignment was completed automatically by the control logic without any time delay.

When the downcomer pressure of the reactor vessel was lower than the specified pressure of 4.03MPa, the SIT started to deliver a high SI flow to the reactor vessel by fully opening the flow control valve. When the water level of the SIT reached a specified point, the stem of the flow control valve was lowered to a specified position to apply more flow resistance to obtain the required low injection flow rate. When the water level of the SIT was lowered to a specified empty set point, the flow control valve was fully closed so that the nitrogen gas could not to be injected into the reactor vessel.

Discharged break flow was transported into a separating vessel of the containment simulator. The separated steam was vented to the atmosphere to maintain a constant pressure in the containment simulator and its flow rate was measured with a vortex flowmeter. The entrained water was separated from the steam at a separator in the separating vessel and then accumulated in one of two measuring vessels by gravity. The accumulated water mass of the measuring vessel was measured by a load cell. The transient was terminated with the termination of the data logging system when it was judged by operators that all the major phenomena had already occurred.

5.4 Major Experimental Results and Analysis

5.4.1 Major Sequence of Events

The major SOE of the SB-DVI-08 test is shown in Table 7. The transient started at 199 seconds. The primary pressure reached a low pressurizer pressure trip set point (LPP) at 219 seconds when the pressurizer pressure decreased to 10.7MPa. The main steam and feedwater lines were isolated after the LPP signal with specified time delays. The core power started to follow the 120% ANS73 curve at 223 seconds. The SIP started to inject ECC water through the DVI-2 nozzle after the LPP signal with a time delay of 28 seconds. Three SITs were activated

Table 7. Major Sequence of Events for the SB-DVI-08 Test

Event	Time (sec)	Remarks
Steady state condition	<199	
Break open	199	
Low pressurizer pressure (LPP)	219	
Main steam isolation	219	
Main feed isolation	226	
Decay power start	223	
SIP	246	
Max. PCT	290	359°C
Loop/downcomer seal clearing	~288	
SIT on	431	
SIT low flow	941/1095/1178	SIT3/SIT1/SIT2
SIT off	4014	SIT3
Stop	4054	

to deliver ECC water through three intact DVI nozzles at 431 seconds: DVI-1, DVI-2, DVI-3. Change from a high to a low flow injection mode of the three SITs occurred between 941 and 1178 seconds. Three SITs showed more or less the same time difference when changing their actuation modes. Eventually, the test was ended at 4054 seconds when there was no significant variation of the major parameters.

5.4.2 Core Power and Peak Cladding Temperature

The ATLAS has a scaled maximum power of 8% of the core power of the APR1400. An initial condition for the SB-DVI-08 test was obtained at 8% core power level by reducing the primary coolant flow rate. This approach enables the ATLAS to have the same temperature distribution along the reactor coolant system as the APR1400. On the initiation of the transient, the core power was maintained at the same level until the core power intersected with the decay power curve of the APR1400. Subsequently, the core power was controlled to follow the 120% ANS73 curve. As mentioned in the previous scaling section, this approach was an optimized one to minimize the inevitable scaling distortion in the ATLAS. Figure 8 shows a variation of the core power together with the power of the MARS code. The measured total core power was larger than the value of the MARS code by the amount of heat loss. The initial heat loss estimated by Eq. (2) was about 88kW, which was approximately 5.6% of the total power. The estimated heat loss was partitioned into three heater groups to give a radially uniform power profile during the transient.

Figure 9 compares the measured PCT with the one predicted by the MARS code. A maximum PCT of 359 °C was observed at around 290 seconds in heater group three, located in the outer region of the core, though the differences among the three heater groups were not very significant due to a depression of the core water level, which causes a core uncovery before a loop seal clearing occurs. The loop seals in the intermediate legs were cleared at around 288 seconds. Though the loop seal clearing was predicted at the similar progression time in the MARS code, the depression of the core water level was not so low as that found in the data. Therefore, an increase in the PCT is not predicted by the MARS code just before the occurrence of a loop seal clearing. A more detailed explanation of core level variation will be described in the following section.

On the other hand, the MARS code predicts a much longer delay for PCT of 470 °C: around 447 seconds at the 16th node of the hot channel, which corresponds to 1.43m from the heated section. This is due to a continuous decrease in the core water level after the occurrence of a loop seal clearing. In the code calculation, a decrease in the core level in the MARS calculation becomes more significant than that predicted by the data, resulting in a longer delayed heat-up of the PCT.

According to a preliminary safety analysis on the

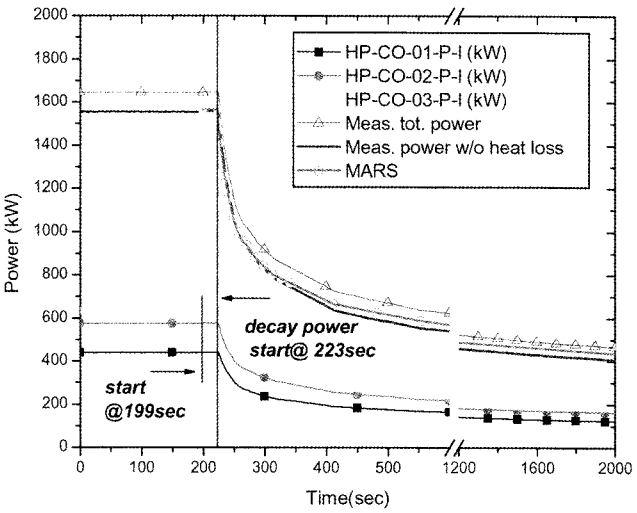

Fig. 8. Comparison of the Core Power Variation During the SB-DVI-08 Test

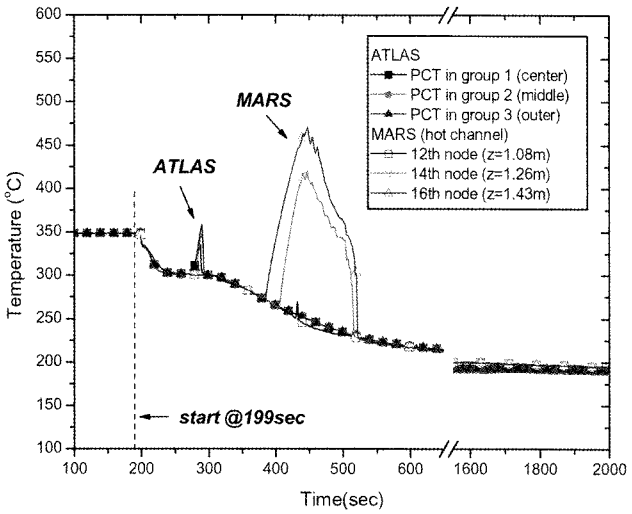

Fig. 9. Comparison of the PCT Behavior During the SB-DVI-08 Test

APR1400, a maximum PCT of 576 °C is predicted for a 100% DVI line break accident [10]. This PCT higher than that in the present data implies that the methodology used for the analysis of the DVI line break accidents of the APR1400 includes more conservatism than does the data.

5.4.3 Pressure Trends

Figure 10 shows the variations of the primary and the secondary pressures during the transient. Predicted pressure trends by the MARS code are also plotted in the same figure. On initiating the break, the primary pressure decreases rapidly due to an abrupt loss of the inventory

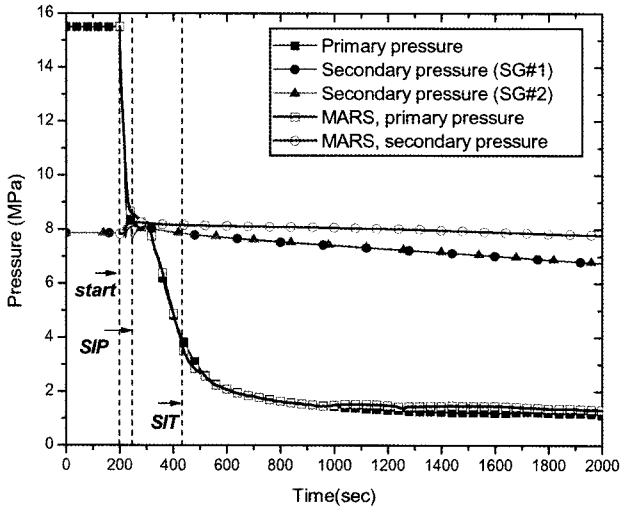

Fig. 10. Comparison of the Primary and the Secondary Pressure During the SB-DVI-08 Test

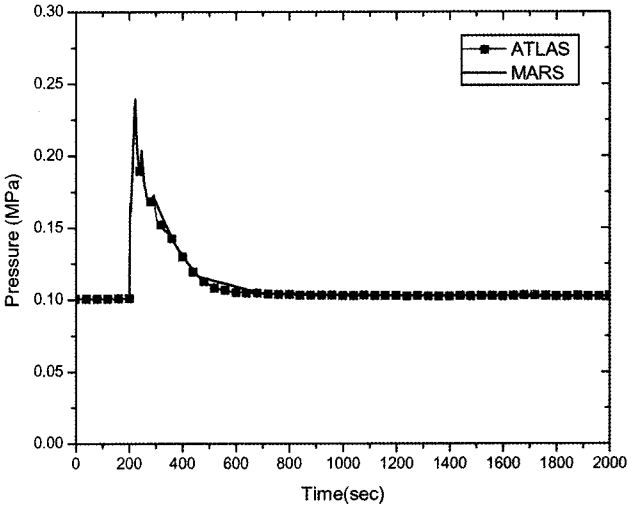

Fig. 11. Comparison of the Containment Pressure During the SB-DVI-08 Test

through the broken DVI-4 nozzle. The decreasing rate of the primary pressure becomes small at around 250 seconds and the primary pressure decreases again. An obvious plateau region of the primary pressure was not observed, implying that the effects of the loop seal on the primary pressure were not so significant in the present test.

In the post-test calculation, a sensitivity study of the discharge coefficient of the break junction was performed to obtain the same primary pressure trend as that found in the data. The Henry-Fauske critical flow model was used as a default model in the MARS calculation. The calculated PCT was affected significantly by the discharge coefficient. It was found that the discharge coefficient of C_d=0.75 at the break nozzle resulted in the best agreement with the data.

The measured secondary pressure reaches a peak of 8.5MPa and then decreases continuously. The secondary pressure was controlled by the operators so as not to reach 9MPa. The MSSV (Main Steam Safety Valve) was opened two times in the early period of the transient. On the other hand, the secondary pressure in the MARS calculation reached the set point of the MSSV and then decreased more slowly than predicted by the data. Overall, the secondary pressure is over-predicted in the MARS calculation during most of the test period. The over-prediction of the secondary pressure by the MARS code seems to be caused by the excessive heat loss to the environment, which occurs on the shell side of the steam generators. A scoping analysis was performed with the MARS code to investigate the effects of the heat loss on the secondary pressure behavior. When an amount of heat loss similar to the primary heat loss is imposed on the shell sides of the steam generators, it is found that the predicted secondary pressure agrees with the measured secondary pressure.

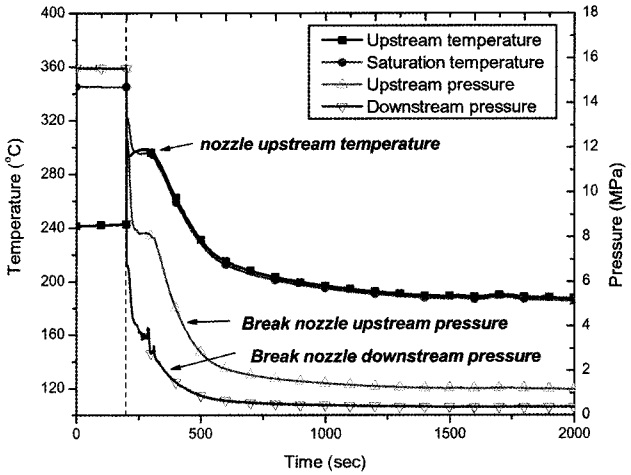

Fig. 12. Pressure and Temperature along the Break Spool Piece During the SB-DVI-08

As for the containment pressure, it increased abruptly up to 0.2MPa due to a considerable initial break flow rate at the initial blowdown period; containment pressure then decreased exponentially to the atmospheric pressure as shown in Fig. 11. The measured containment pressure was used as a boundary condition in the post-test calculation.

5.4.4 Choking Characteristics

A special break spool piece was fabricated and installed at the DVI-4 nozzle to simulate a guillotine break of a DVI line. The piece consists of a break nozzle, a break nozzle case, a quick opening gate valve, and instruments as shown in Fig.3. The break nozzle was designed according to the scaling law so that a scaled-down break

flow rate escapes from the primary system. The quick opening valve was triggered within 0.5 seconds as expected.

The pressures and temperatures upstream and downstream of the break spool piece were measured simultaneously. A variation of both upstream and downstream pressures of the break spool piece is shown in Fig. 12, along with the temperature trend. Choking was maintained throughout the test period due to the considerable pressure difference across the break nozzle. The ratio of the downstream to the upstream pressure of the break spool piece decreases to a value less than 0.6 within a few seconds of the break. The pressure ratio continuously decreases to 0.32 at about 400 seconds and maintains an almost constant value. A subcooled break flow was observed in the early period of the test as seen in Fig.12. However, the break flow changed rapidly to a saturated break flow condition and maintained a saturated choking condition during the remaining test period.

5.4.5 Break Flow Characteristics

The containment simulating system of the ATLAS is such that a two-phase break flow is separated into a separating vessel and each separated flow rate is measured by different measurement techniques [5]. Once a two-phase break flow is introduced into the separating vessel, it should be completely separated into vapor and water within the separating vessel. Then, the separated vapor and water should be transported to each flow rate measuring system, the vortex flowmeter for vapor and the load cell for water. It was found that the separated vapor flow rate can be measured reasonably well by the flowmeter, but that the water flow rate was not measured reliably, especially for a flow rate higher than about 4kg/s. It took a certain delay time for the separated water to be drained to the measuring vessel, where the drained water was weighed by a load cell. The main cause for the delayed drain of the water was identified to be a swirling water flow inside the separating vessel. This swirling effect was accelerated by the separated, high velocity, vapor flow. Eventually, the separated water continued whirling in the separating vessel, resulting in a periodic water level fluctuation. It was also found that this water swirling tended to become significant as the break flow rate became higher. As a consequence, it has been concluded that the existing break flow measurement system has a definite limitation for measuring separated water flow rate and that system design needs to be improved for a more reliable measurement.

So, several design modifications have been made to the separating vessel to drain the separated water efficiently to the measuring vessel. The hemispheric bottom part of the separating vessel was reconstructed to be a cone-shape with an enlarged diameter; several rib-like plates were vertically installed inside the vessel to prevent the water swirling effect. It was found from several characteristic tests that this modification considerably reduced water accumulation inside the separating vessel, leading to much improved break flow measuring performance.

As an alternative to the present method, the load cell-based break flow measuring method, an RCS inventory-based break flow estimation method, has been developed to obtain a more accurate break flow rate, especially in the initial stage of the selected transient. This method is based on a mass balance of the reactor coolant inventory between a change in the RCS inventory and the ECC injection flow rate during the progression of the break. The mass balance of the primary reactor coolant inventory can be expressed by

$$W_{Break} = W_{ECC} - \frac{dM_{RCS}}{dt}, \tag{3}$$

where W_{Break} and W_{ECC} are the break flow rate and the ECC water flow rate, respectively. M_{RCS} is the RCS water inventory. An accumulated break flow is obtained by an integration of the mass balance equation as follows:

$$\int_0^t W_{Break}\,dt = \int_0^t W_{ECC}\,dt + M_{RCS}^{(0)} - M_{RCS}^{(t)} \tag{4}$$

The RCS coolant inventory is distributed into several sub-systems such as the reactor core, the downcomer, the hot legs, the cold legs, the intermediate legs, the pressurizer, etc. The primary coolant system was divided into a total of 30 sub-systems in the present method. The total RCS coolant inventory can be obtained by summing all the coolant masses of the 30 sub-systems. The coolant mass of each sub-system can be obtained by considering the coolant density and volume as follows:

$$M_{RCS}^{(t)} = \sum_{i=1}^{n}\left(\rho_i^{(t)} \cdot V_{RCS,i}^{(t)}\right), \tag{5}$$

where the subscript i indicates an index for a sub-system composing the primary system of the ATLAS. The coolant volume of each sub-system $V_{RCS,i}$ is obtained from the measured water level in that sub-system. An empirical volume table correlating water volume and water level for a certain sub-system was obtained by separate inventory tests. A total of twelve empirical volume tables were created and the same tables were applied to the sub-systems, which were geometrically symmetrical to each other. The other influencing parameter used to calculate the coolant mass of a divided sub-system is the coolant density, which is expected to vary during the transient. Therefore, a reference pressure and temperature are necessary to calculate average coolant density for each sub-system. In order to represent the mean pressure and temperature in each sub-system, reference pressure and

Table 8. Summary of the Sub-systems Consisting of the Primary Coolant System and the Reference Tags

No	Sub-system	Empirical volume table	Reference tags (pressure/temp.)
1	Reactor pressure vessel	RPVtable	PT-UH-03/TF-LP-02G18
2	Downcomer	DCtable	PT-DC-01/TF-DC-022
3	Upside of the U-tube of SG 1	SGUtable	PT-DC-01/TF-SGP1-01
4	Upside of the U-tube of SG 2		PT-DC-01/TF-SGP2-01
5	Downside of the U-tube of SG 1		PT-DC-01/TF-SGP1-02
6	Downside of the U-tube of SG 1		PT-DC-01/TF-SGP2-02
7	Inlet plenum of SG 1	SGIPtable	PT-DC-01/TF-SGP1-01
8	Inlet plenum of SG 2		PT-DC-01/TF-SGP2-01
9	Outlet plenum of SG 1	SGOPtable	PT-DC-01/TF-SGP1-02
10	Outlet plenum of SG 2		PT-DC-01/TF-SGP2-02
11	Hot leg of the loop 1	HLtable	PT-UH-01/TF-HL1-03A
12	Hot leg of the loop 2		PT-UH-01/TF-HL2-03A
13	Cold leg 1A of loop 1	CLtable	PT-DC-01/TF-CL1A-04A
14	Cold leg 1B of loop 1		PT-DC-01/TF-CL1B-04A
15	Cold leg 2A of loop 2		PT-DC-01/TF-CL2A-04A
16	Cold leg 2B of loop 2		PT-DC-01/TF-CL2B-04A
17	Downward interm. leg 1A of loop 1	IL1table	PT-DC-01/TF-IL1A-01A
18	Downward interm. leg 1B of loop 1		PT-DC-01/TF-IL1B-01A
19	Downward interm. leg 2A of loop 2		PT-DC-01/TF-IL2A-01A
20	Downward interm. leg 2B of loop 2		PT-DC-01/TF-IL2B-01A
21	Horizontal interm. leg 1A of loop 1	IL2table	PT-DC-01/TF-IL1A-02A
22	Horizontal interm. leg 1B of loop 1		PT-DC-01/TF-IL1B-02A
23	Horizontal interm. leg 2A of loop 2		PT-DC-01/TF-IL2A-02A
24	Horizontal interm. leg 2B of loop 2		PT-DC-01/TF-IL2B-02A
25	Upward interm. leg 1A of loop 1	IL3table	PT-DC-01/TF-IL1A-03A
26	Upward interm. leg 1B of loop 1		PT-DC-01/TF-IL1B-03A
27	Upward interm. leg 2A of loop 2		PT-DC-01/TF-IL2A-03A
28	Upward interm. leg 2B of loop 2		PT-DC-01/TF-IL2B-03A
29	Pressurizer	PZRtable	PT-PZR-01/TF-PZR-01
30	Hot leg to pressurizer surge line	HL2PZRtable	PT-PZR-01/TF-SUR-01

temperature were determined carefully from among the several instruments installed within each sub-system. As the pressure distribution was almost uniform along the primary system, either the RPV upper head pressure, the downcomer pressure, or the pressurizer pressure was selected as a reference pressure for each divided sub-system. Reference temperature was determined more carefully from among the available temperature signals within each sub-system; otherwise, the vapor density can be obtained when the temperature is close to a saturated condition. Consequently, the transient RCS inventory was calculated indirectly by taking account of both the measured water level and the representative density of each sub-system. Once the transient RCS inventory was obtained, a break flow rate was achieved with the measured ECC flow rate. A list of the divided sub-systems and the reference pressures and temperatures used for the density calculation are summarized in Table 8.

A comparison of the three measured break flow rates with the one predicted by the MARS code is shown in

Fig. 13; (1) existing load cell-based measurement (2) modified load-cell based measurement (3) RCS inventory-based measurement. The existing load cell-based break flow result, which was carried out before the separating vessel was improved, was plotted together with the present results for comparison. The unphysical peak around 600 seconds is due to drainage of the accumulated water by swirling motion in the separating vessel. It can be seen from Fig. 13 that the present modification of the separating vessel results in much improved break flow measurement results, especially for the early blowdown period. Delayed drainage of the separated water also disappeared in the modified measurement system.

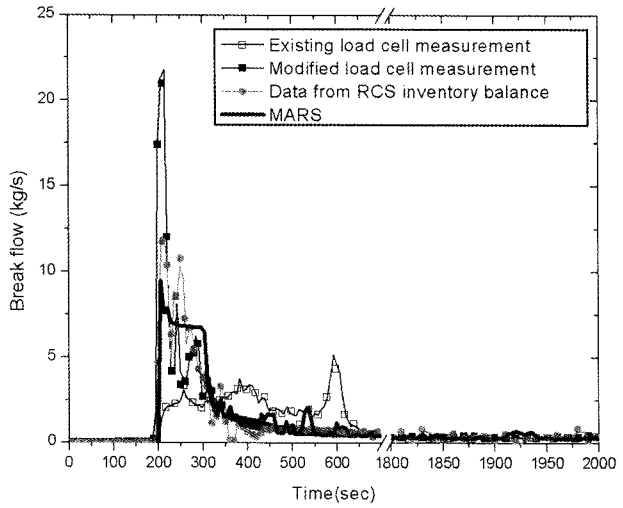

Fig. 13. Comparison of the Break Flow During the SB-DVI-08

The RCS inventory-based break flow shows results closer to the values predicted by the MARS code than the modified load cell-based break flow. The initial peak during the blowdown period is between the modified load-cell based value and the calculation. The initial peak from the modified load cell-based measurement seems to be over-estimated slightly because an abrupt pressure increase in both the separating vessel and the measuring vessel during the blowdown period provides an additional load on the load cell. This over-estimation of the break flow can be seen by a comparison of the measured accumulated break flow with the value predicted by the MARS code, and is shown in Fig 14. The initial slope for the modified load cell-based measurement is the steepest among the other cases. Thus, the RCS inventory-based break flow rate provides a more reliable break flow than the modified load cell-based break flow, especially for the early period of the transient. Apart from the initial period, the modified load cell-based measurement and the RCS inventory-based measurement provide very consistent results. Overall the MARS code predicts the accumulated break flow reasonably well.

5.4.6 ECC Water Flow and Mass Balance

During the present guillotine break test of a DVI line, ECC water was provided by one SIP and three SITs with a single failure assumption. One safety injection pump was initiated at 246 seconds with a time delay of 28.28 seconds after the primary pressure reached 10.72MPa. The delay time was determined by applying a time scaling ratio of the ATLAS to the delay time of the reference plant, APR1400. In the meantime, three safety injection tanks started to deliver ECC water through the three intact DVI nozzles when the downcomer pressure reached

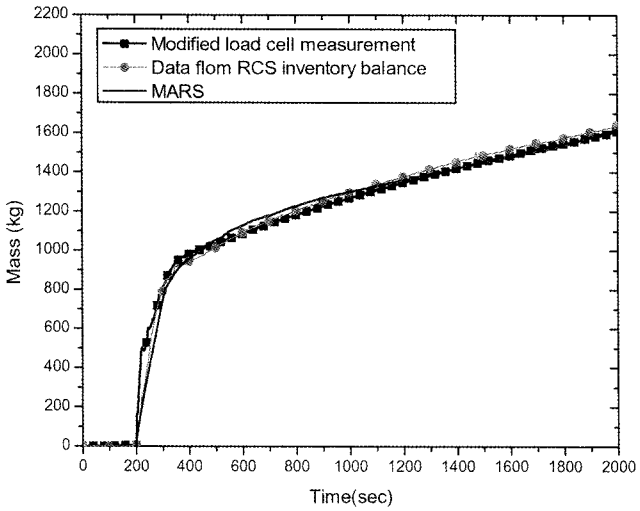

Fig. 14. Comparison of the Accumulated Break Flow During the SB-DVI-08

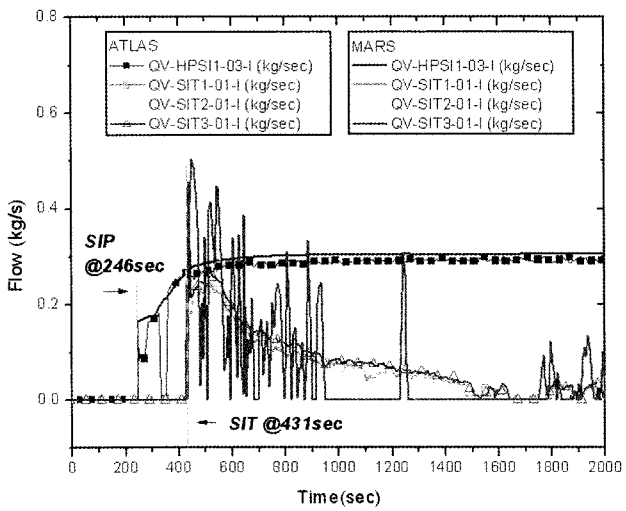

Fig. 15. Comparison of the ECC Water Flow During the SB-DVI-08

4.03MPa at 431 seconds. A comparison of the ECC water flow with the results calculated by the MARS code is shown in Fig. 15. The actuation times for the SIP and SITs predicted by the MARS code are very consistent with the present data as the primary pressure is reproduced well by the code. The calculated ECC water flow rate by the SIP agrees with the measured data. There was an inadvertent closure of the isolation valve downstream of the SIP for 20 seconds at about 330 seconds, which caused failure of ECC injection. But, this was found not to be significant in the progression of the major transient. Three SITs provided almost the same ECC injection flow rate from the actuation time of 431 seconds. However, the MARS code predicts an oscillatory behavior for the ECC water flow rate by the SIT. Accumulated ECC water mass injected into the primary system during the transient is compared with that predicted by the MARS calculation in Fig. 16. The prediction of the accumulated ECC water by the SIP is slightly higher than the data. The predicted ECC flow by the SITs is slightly higher than the data until 1100 seconds and is slightly lower than the data during the remaining period of the transient. Overall the MARS code predicts the accumulated ECC water mass with reasonable accuracy.

Comparison of an accumulated mass balance during the present test is plotted in Fig. 17. Accumulated break flow and ECC water flow are compared with the calculation results. Overall, the prediction by the MARS code is in reasonable agreement with the data, even though a little disagreement exists in the accumulated break flow between the calculation and the experimental data, especially in the early period of the transient.

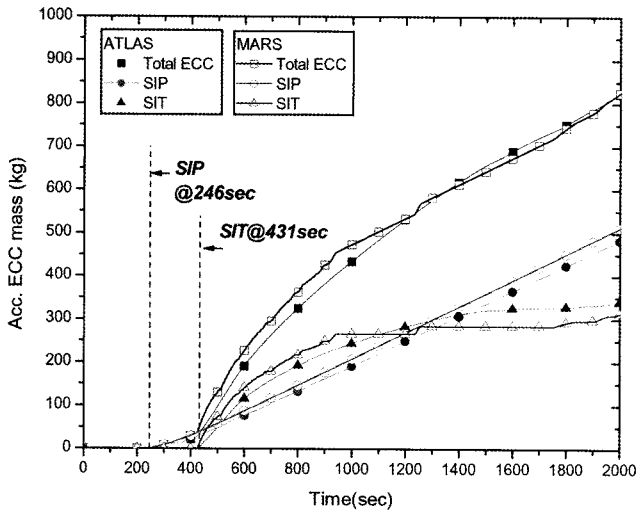

Fig. 16. Comparison of the Accumulated ECC Water During the SB-DVI-08

5.4.7 Core and Downcomer Collapsed Water Level

A comparison of the collapsed water level of the core with the level predicted in the calculations is shown in Fig. 18. The measured collapsed water level of the core decreased to about 30% of the active core region as soon as the break occurred, thereby causing the PCT to increase. Such initial core level decreases were recovered when the loop seals in the intermediate legs were cleared. The MARS code predicts a similarly decreased level in the very early period of the transient but this decreased level is not as low as that found in the measured data. This difference is the main reason why no increase in the PCT

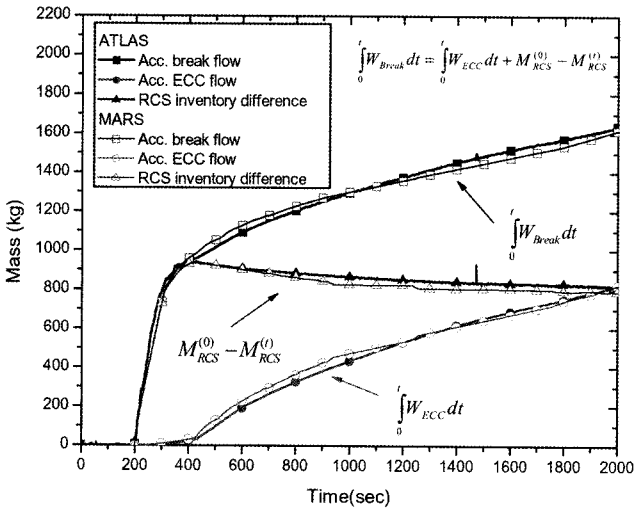

Fig. 17. Comparison of the Accumulated Mass Balance During the SB-DVI-08

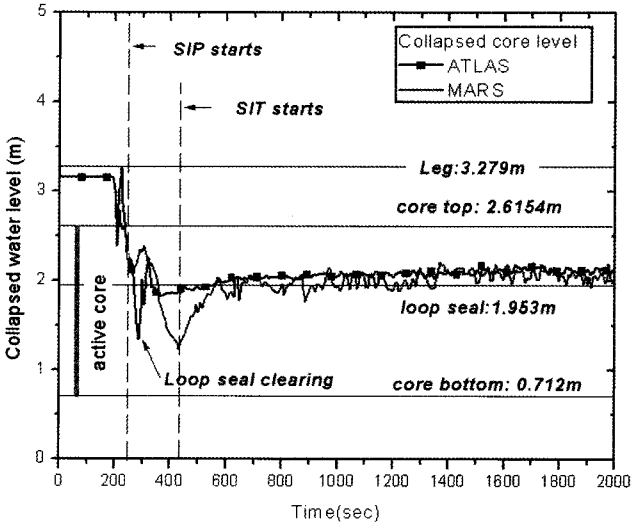

Fig. 18. Comparison of the Collapsed Core Water Level During the SB-DVI-08

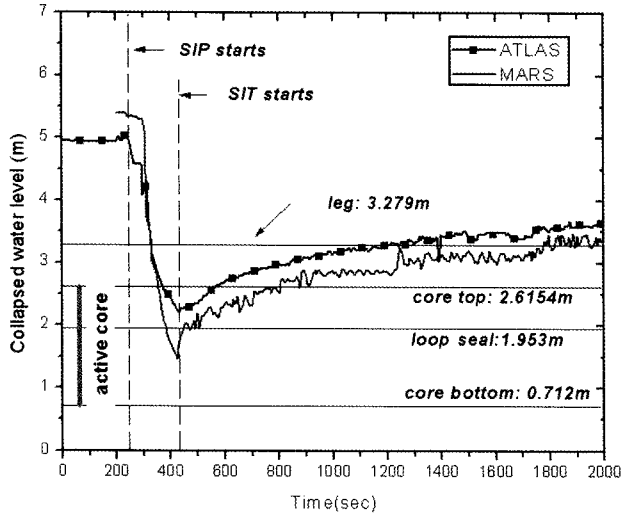

Fig. 19. Comparison of the Collapsed Downcomer Water Level During the SB-DVI-08

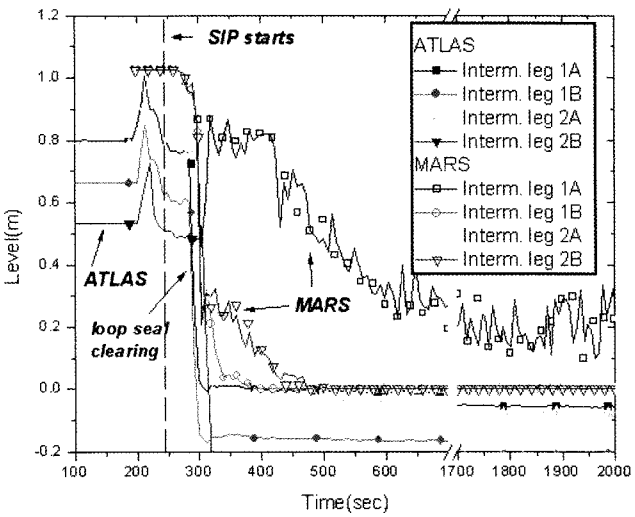

Fig. 20. Comparison of the Collapsed Level in the Vertical Intermediate Leg During the SB-DVI-08

is predicted, as shown in Fig. 9. This disagreement is supposed to be caused by uncertainties in predicting countercurrent flow or condensation phenomena in a downcomer region, which were ranked high in the PIRT process.

Subsequent to the loop seal clearing, the collapsed water level of the core shows a continuous decrease until the SIT starts to inject additional ECC water into the core. This level decrease is attributed to the fact that the break flow rate is greater than the ECC water flow rate by the SIP during the period when the SITs are not working. When the SITs start to inject ECC water into the core, the collapsed water level of the core is recovered. However, the MARS code predicts a more rapid decrease in the collapsed water level of the core during the period between the loop seal clearing and the SIT actuation than does the data, leading to the delayed increase in the PCT shown in Fig. 9. This is due to the fact that the predicted break flow is larger than that shown in the data during that period, as shown in Fig. 17.

A comparison of the measured downcomer collapsed water level with the calculated level is shown in Fig. 19. On a break initiation, the downcomer collapsed water level decreases continuously. It was not until the SITs started to deliver ECC water into core that the downcomer collapsed water level started to recover. The calculated water level shows a more rapid decreasing trend than predicted by the data during the post-trip phase before the actuation of the SITs.

5.4.8 Loop Seal Phenomena

A blockage of the primary coolant loop with water filled at the intermediate legs, denoted as a "loop seal," is expected to have a significant influence on the core cooling

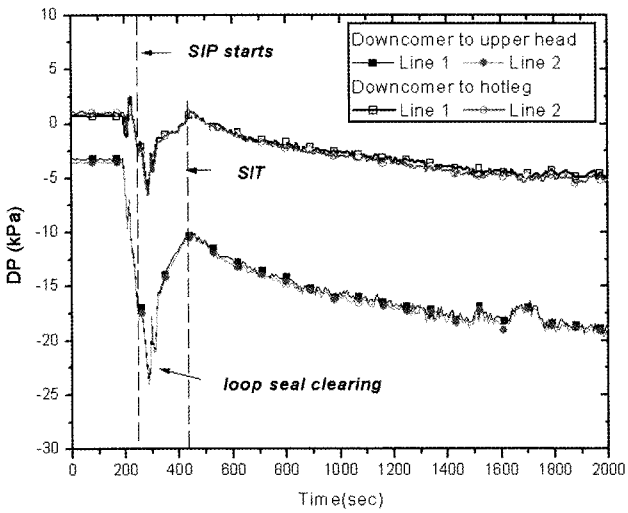

Fig. 21. Measured Pressure Drop Across the Core Bypass Lines During the SB-DVI-08

phenomena during a DVI line break accident. The core cooling capability is considered to be degraded during this loop seal period because the core water level is decreased considerably. When the loop seal is cleared, the core water level recovered rapidly and the primary pressure fell below that of the secondary side pressure. Consequently, the direction of the heat transfer is reversed and the steam generator begins to supply heat to the primary side. Figure 20 shows the variation of the collapsed water level of the vertical intermediate legs, which is indicative of the occurrence of a loop seal clearing. Two loop seals of loop 2 were cleared simultaneously at 280

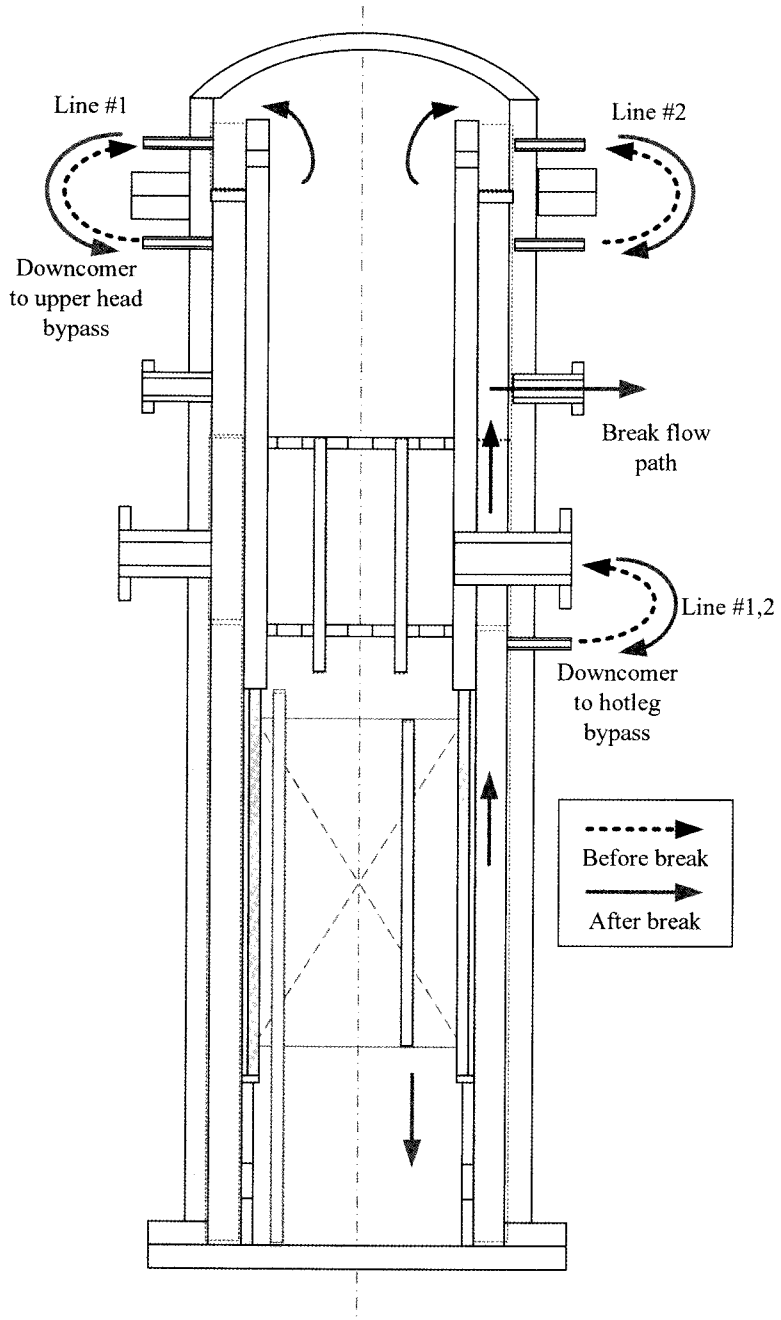

Fig. 22. Schematic Diagram of the Primary Flow Paths During the SB-DVI-08

seconds, followed by a clearing of the other two loop seals of loop 1 at 290 seconds. The difference in the occurrence time of the loop seal clearings between the loop 1 and 2 seems to be due to a non-uniform azimuthal water level distribution in the annulus downcomer region. In the MARS calculation, three loop seals were cleared simultaneously, almost at the same time as the test, whereas the loop seal of loop 1A was cleared in a very gradual manner. Such gradual occurrence of the loop seal clearing of loop 1A is due to an asymmetry effect in the azimuthal direction. Thus, the MARS code predicts more noticeable asymmetric behavior for the loop seal clearing phenomena than does the data.

Figure 21 shows the measured pressure drop across the core bypass lines during the present test. As described in the previous section, two bypass flow paths in the

reactor pressure vessel were simulated with control valves; one is from the downcomer to the upper head; the other is from the downcomer to the hot leg. Each bypass flow path consists of two separate external lines. A schematic diagram of the bypass flow paths is shown in Fig. 22. During a steady state condition before the break, a portion of the core flow is bypassed from the downcomer to the upper head as well as the hot leg, resulting in a positive pressure drop, as shown in Fig.21. The small negative pressure drop along the path from the downcomer to the upper head seems to be due to a biased error of the pressure transmitter. After the break, the direction of the bypass flow is reversed because the primary coolant inventory is discharged through the broken DVI nozzle located at the upper downcomer. This reversed bypass flow causes a negative pressure drop, as depicted in Fig. 22. The pressure drops along the bypass flow paths decreased to a large negative value until a loop seal clearing occurred at about 290 seconds. After the loop seal clearing, the pressure drop increased due to a decreased break flow rate. The pressure drop started to decrease again when the SIT was initiated to inject the ECC water into the downcomer. The injection of the ECC water had a decreasing effect on the quality of the two-phase mixture of the bypass flow. That is the main reason for the large negative pressure drop observed after the initiation of the SITs.

6. CONCLUSION AND RECOMMENDATIONS

The first-ever integral effect test for simulating a 100% DVI line of the APR1400 was carried out with the ATLAS (Advanced Thermal-hydraulic Test Loop for Accident Simulation) from the same prototypic pressure and temperature conditions as found in the APR1400. A scaling analysis was performed on the crucial components, whose performance can influence transient behavior, to determine the initial and boundary conditions for a DVI line break test.

Three phases, except for the long term cooling phase defined in the PIRT, for a DVI line break accident were simulated successfully: pre-trip, post-trip, and refill phases. Rapid depressurization took place during the pre-trip phase, which lasted for 20 seconds. During the post-trip phase, the collapsed water level in the core decreased considerably before a loop seal clearing, so that a core uncovery occurred, resulting in a rapid increase in the PCT even though ECC water was injected into the core from a safety injection pump (SIP). All four loop seals were cleared almost at the same time and the primary pressure started to decrease again from a pressure plateau region. It was observed that the ECC water provided by one SIP was not enough to prevent the downcomer water level from decreasing. Not until the refill phase in which the SITs started to deliver ECC water into core did the downcomer collapsed water level start to recover.

A post-test calculation was performed with a best-estimated thermal hydraulic safety analysis code, MARS 3.1. Overall, the MARS code revealed reasonable prediction results for the present data. However, it was found that a noticeable disagreement exists in the core water level, especially just before a loop seal clearing occurs. This is considered to be the main reason why no increase in the PCT is predicted. It seems that the thermal hydraulic behavior occurring at the downcomer region before a loop seal clearing is not predicted appropriately by the MARS code. This might be due to a deficiency in the relevant models of the MARS code, which describe thermal-hydraulic behavior in the annulus downcomer region such as countercurrent flow and condensation. Besides, a nodalization method of the downcomer region may affect the prediction results. The present integral effect test data will be used to evaluate the prediction capability of the MARS code and to identify any code deficiencies for DVI line break accidents. Furthermore, the present database will be useful in supporting the present conservative safety analysis methodology and developing a new best-estimate safety analysis methodology for DVI line break accidents of the APR1400.

ACKNOWLEDGMENTS

This work has been carried out under the support of the Ministry of Education, Science and Technology (MEST) of the Korean government, under the national nuclear mid- & long-term R&D program.

REFERENCES

[1] W. P. Baek, C.-H. Song, B. J. Yun, T. S. Kwon, S. K. Moon and S. J. Lee, "KAERI Integral Effect Test Program and the ATLAS Design," *Nucl. Technol.*, **152**, 183 (2005).

[2] W. P. Baek and Y. S. Kim, "Accident Simulation ATLAS for APWRs," *Nuclear Engineering International*, **53**, 21 (2008).

[3] K. Y. Choi, H. S. Park, D. J. Euh, T. S. Kwon and W. P. Baek, "Simulation Capability of the ATLAS Facility for Major Design-Basis Accidents," *Nucl. Technol.*, **156**, 256 (2006).

[4] Y. S. Kim, W. P. Baek, C.-H. Song, K. Y. Choi, H. S. Park, S. Cho, K. H. Kang, B. D. Kim, S. K. Moon, B. J. Yun, C. H. Chung, T. S. Kwon, D. J. Euh, N. H. Choi, J. K. Park, and K. H. Min, "Startup Test Report of ATLAS," KAERI/TR-3330/2007 (2007).

[5] K. Y. Choi, H. S. Park, S. Cho, D. J. Euh, Y. S. Kim and W. P. Baek, "Integral Behavior of the ATLAS Facility for a 3-inch Small Break Loss of Coolant Accident," *Nuclear Engineering and Technology*, **40**, 199 (2008).

[6] H. S. Park, K. Y. Choi, S. Cho, K. H. Kang, N. H. Choi, E. J. Euh, Y.S. Kim and W. P. Baek, "An Integral Effect Test on the Reflood Period of a Large-Break LOCA for the APR1400 Using the ATLAS," Proc. of ICAPP'08, Anaheim, CA, USA, June 8-12 (2008).

[7] C.-H. Song, T. S. Kwon, H. J. Chung, C. K. Park, C. H. Chung, S. Y. Chun and J. -K. Park, "Thermal Hydraulic

Test Program for Evaluating or Verifying the Performance of New Design Features in KNGR," Proc. of Korean Nuclear Society Autumn Meeting, Daejeon, Korea (2000).
[8] B. J. Yun, C. H. Song, K. H. Min, H. K. Cho and G. C. Park, "Experimental Observations of the Hydraulic Phenomena in the APR1400 Downcomer during the DVI Line Break Accident," Proc. of Korean Nuclear Society Spring Meeting, Gyeongju, Korea (2003).
[9] EPRI, "EPRI Utility Requirement Documents for the Advanced Light Water Reactor (Chapter 5)," (1995).
[10] Korea Electric Power Co., "Shin-Kori Unit 3&4 Preliminary Safety Analysis Report," (2003)
[11] K. H. Bae, H. S. Lim, J. H. Song, S. K. Sim and J. K. Park, "Design Options for the Safety Injection System of Korean Next Generation Reactor," *Annals of Nuclear Energy*, **27**, 1011 (2000).
[12] B. D. Chung, S. J. Lee, W. P. Baek, J. H. Song, Y. S. Bang, H. G. Kim, S. J. Lee, S. Y. Lee, "Phenomena Identification and Ranking Tabulation for APR1400 Direct Vessel Injection Line Break," The 10th Int. Topical Meeting on Nuclear Reactor Thermal Hydraulics (NURETH-10), Seoul, Korea, Oct.5-9 (2003).
[13] B. U. Bae, K. H. Lee and G. C. Park, "Integral Experiment and RELAP5 Analysis for DVI line Break SBLOCA in APR1400," Proc. of ICAPP 2007, Nice, France, May 13-18 (2007).
[14] M. Ishii and I. Kataoka, "Similarity Analysis and Scaling Criteria for LWRs Under Single Phase and Two-Phase Natural Circulation," NUREG/CR-3267, ANL-83-32, Argonne National Laboratory (1983).
[15] H. S. Park, S. K. Moon, B. J. Yun, T. S. Kwon, K. Y. Choi, C. K. Park, S. Cho, S. D. Hong, S. J. Yi, Y. S. Kim, C.-H. Song, and W. P. Baek "Calculation Sheet for the Basic Design of the ATLAS Fluid System," KAERI/TR-3333/2007 (2007).
[16] J. H. Lienhard, "On the Commonality of Equations for Natural Convection from Immersed Bodies," *Int. J. Heat Mass Transfer*, **16**, 2121 (1973).
[17] H. K. Fauske, "The Discharge of Saturated Water through Tubes," *Chemical Engineering Progress Symposium Series*, **61**, 210 (1965).
[18] M. H. Chun and C. K. Park, and J. W. Park, "An Experimental Investigation of Critical Flow Rates of Subcooled Water Through Short Pipes with Small Diameters," *Int. Comm. Heat Mass Transfer*, **23**, 1053 (1996).
[19] I. C. Chu, C.-H. Song, B. H. Cho and J. K. Park, "Development of Passive Flow Controlling Safety Injection Tank for APR1400," Nuclear Engineering and Design, 238, 200 (2007).
[20] K. Y. Choi, Y. S. Kim, S. J. Yi, W. P. Baek, "Development of a Pump Performance Model for an Integral Effect Test Facility," *Nuclear Engineering and Design*, **238**, 2614 (2008).